Atmos. Meas. Tech. Discuss., 8, 6559–6597, 2015
www.atmos-meas-tech-discuss.net/8/6559/2015/
doi:10.5194/amtd-8-6559-2015


Atmospheric Measurement Techniques Discussions



# A better understanding of POLDER's cloud droplet size retrieval: impact of cloud horizontal inhomogeneity and directional sampling

**H. Shang[1,2], L. Chen[1], F.-M. Bréon[3], H. Letu[4], S. Li[1], Z. Wang[5], and L. Su[1]**

[1]State Key Laboratory of Remote Sensing Science, Institute of Remote Sensing and Digital Earth, Chinese Academy of Sciences, Beijing, China
[2]University of the Chinese Academy of Sciences, Beijing, China
[3]Laboratoire des Sciences du Climat et de l'Environnement, UMR CEA-CNRS-UVSQ, Gif-Sur-Yvette, France
[4]Research and Information Center, Tokai University, Tokyo, Japan
[5]Satellite Environment Center, Ministry of Environmental Protection, Beijing, China

Received: 17 May 2015 – Accepted: 08 June 2015 – Published: 01 July 2015

Correspondence to: L. Chen (chenlf@radi.ac.cn)

Published by Copernicus Publications on behalf of the European Geosciences Union.







## Abstract

The principles of the Polarization and Directionality of the Earth's Reflectance (POLDER) cloud droplet size retrieval requires that clouds are horizontally homogeneous. Nevertheless, the retrieval is applied by combining all measurements from an area of 150 km × 150 km to compensate for POLDER's insufficient directional sampling. Using the POLDER-like data simulated with the RT3 model, we investigate the impact of cloud horizontal inhomogeneity and directional sampling on the retrieval, and then analyze which spatial resolution is potentially accessible from the measurements. Case studies show that the sub-scale variability in droplet effective radius (CDR) can mislead both the CDR and effective variance (EV) retrievals. Nevertheless, the sub-scale variations in EV and cloud optical thickness (COT) only influence the EV retrievals and not the CDR estimate. In the directional sampling cases studied, the retrieval is accurate using limited observations and is largely independent of random noise.

Several improvements have been made to the original POLDER droplet size retrieval. For example, the measurements in the primary rainbow region (137–145°) are used to ensure accurate large droplet (> 15 µm) retrievals and reduce the uncertainties caused by cloud heterogeneity. We apply the improved method using the POLDER global L1B data for June 2008, the new CDR results are compared with the operational CDRs. The comparison show that the operational CDRs tend to be underestimated for large droplets. The reason is that the cloudbow oscillations in the scattering angle region of 145–165° are weak for cloud fields with CDR > 15 µm. Lastly, a sub-scale retrieval case is analyzed, illustrating that a higher resolution, e.g., 42 km × 42 km, can be used when inverting cloud droplet size parameters from POLDER measurements.





AMTD
8, 6559–6597, 2015



## 1 Introduction

Liquid water clouds cover approximately 20–30 % of the globe and play an important role in the Earth's radiation balance (Zeng et al., 2011). The radiative properties of liquid water clouds depend on their droplet size distributions, which are represented by the droplet effective radius (CDR) and the effective variance (EV) (Breon and Doutriaux-Boucher, 2005; Bréon and Colzy, 2000; Hansen and Travis, 1974). The parameterization of droplet size distributions in climate models has been found to be important for evaluating global climate change (Liu et al., 2002, 2011). Hence, the observation of CDR and EV not only has a significant influence on the modeling of liquid clouds' climate feedbacks (Stubenrauch et al., 2013; Dandin et al., 1997) but is also meaningful to aerosol-cloud-precipitation interaction research (Penner et al., 2004; Shang et al., 2014). Satellite measurements of the CDR and EV have been used to extend the detailed knowledge gained from specific cloud campaign studies to the larger spatial and temporal scales that are relevant to climate.

Remote sensing of droplet size distribution is achieved either through the bi-spectral reflectance method or the multi-angular polarized reflectance method. Nakajima and King (1990) introduced the bi-spectral reflectance method. This approach is based on the measured bi-spectral reflectance in the visible and near-infrared bands, which are jointly sensitive to cloud optical thickness and particle size. In the shortwave infrared, absorption increases with the droplet size, so that the cloud reflectance is lower for larger cloud CDRs. The reflectance measurements at 1.6, 2.1 and 3.7 µm are compared to those in the near-IR using pre-calculated look-up tables (LUT) to derive the cloud optical thickness and the CDR. This method has been used to derive daytime CDR from the Global Retrieval of ATSR Cloud Parameters and Evaluation (ATSR-GRAPE), the Pathfinder Atmospheres Extended (PATMOS-x), the Visible Infrared Imaging Radiometer Suite (VIIRS), the National Oceanic and Atmospheric Administration/Advanced Very-High-Resolution Radiometer (NOAA/AVHRR) (Nakajima and Nakajima, 1995; Kawamoto et al., 2001) and the Moderate-Resolution Imaging





AMTD
8, 6559–6597, 2015



Spectroradiometer (Baum et al., 2000; Platnick et al., 2003; Sayer et al., 2011; Walther and Heidinger, 2012). Nighttime cloud properties have been derived from the reflected moonlight as measured by the VIIRS instrument (Walther et al., 2013).

Although the bi-spectral method is well established and widely used, it still suffers from significant limitations. In particular, it cannot provide useful information on the EV which is assumed in the computation of the LUT. For instance, the MODIS algorithm assumes EV = 0.1. In reality, the cloud EV changes with cloud type (Zhang, 2013), and the EV of many stratocumulus cloud fields is found to be equal to or less than 0.05 (Breon and Doutriaux-Boucher, 2005). In addition, the LUT are calculated for a plane-parallel cloud field using a 1-D radiative transfer model, which does not consider the influence of the 3-D structure of clouds. Nevertheless, Horváth (2004) found that no more than 17 % of marine liquid water clouds pixels are plane-parallel objects, suggesting that the retrieval error arising from the solar-viewing geometry cannot be neglected (Zinner et al., 2010; Wolters et al., 2010; Vant-Hull et al., 2007; Di Girolamo et al., 2010). Effects of cloud horizontal homogeneity also make the retrieval more complex. Marshak et al. (2006) found that ignoring the cloud variability at the sub-pixel scale causes an underestimate of the CDR, while ignoring cloud inhomogeneity at scales exceeding the pixel scale can lead to overestimates. Zeng et al. (2011) reported that the vertical structure induced by drizzle and 3-D radiative effects operate together to cause dramatic differences between 1.6, 2.1 and 3.7 µm retrievals (Zhang et al., 2012; Zhang, 2013; Nakajima et al., 2010a, b; Nagao et al., 2013). In addition, the water vapor absorption within a cloud and the presence of an absorbing aerosol layer above a cloud leads to a positive bias in the retrieval (Alexandrov et al., 2012; Coddington et al., 2010; Haywood et al., 2004).

The multi-angular polarized method (Bréon and Goloub, 1998) was developed for the Polarization and Directionality of the Earth's Reflectance (POLDER) instrument. The polarized radiance observed by the satellite is a function of cloud microphysical properties, e.g., particle shape and effective radius (Goloub et al., 2000). In the scattering angle range of 135 to 165° (the rainbow region), the polarized reflectance in





AMTD
8, 6559–6597, 2015



the non-absorbing visible and infrared bands exhibits several peaks and troughs, i.e., supernumerary cloudbow. The angular positions of these peaks are exclusively sensitive to CDR; moreover, the polarization amplitudes are sensitive to the EV (Bréon and Colzy, 2000), allowing the CDR and EV to be determined simultaneously. The polarized reflectance is proportional to the polarized phase function (the phase matrix elements $P_{12}$ computed using Mie theory). Therefore, in the retrieval, the CDR and EV are derived simultaneously by matching the satellite-measured polarized reflectance curve to pre-computed polarized phase functions. The polarized component of the upwelling radiance is dominated by the upper layer of the cloud field; the signal tends to saturate for cloud optical thicknesses greater than 2–3 (Bréon and Goloub, 1998; Goloub et al., 2000). The structures of the rainbow and supernumerary bows are determined by the single scattering properties of spherical droplets. Surface albedo (surface type) can then be omitted in the retrieval algorithm (Breon and Doutriaux-Boucher, 2005). Alexandrov et al. (2012) assessed the accuracy of the polarized technique with a research scanning polarimeter (RSP), which is an airborne prototype for the Aerosol Polarimeter Sensor (APS, part of the Glory Project) satellite. Furthermore, sensitivity studies have been conducting regarding the effects of 3-D radiative transfer, solar-viewing geometry, aerosol layers above clouds, and two-layer clouds, demonstrating that the polarized technique is robust. The same paper analyses the range of scattering angle range viewed by the APS that depends on the solar-viewing geometry. Radiative transfer simulations indicate that the retrieved effective variance tends to be overestimated due to the smoothing effect of multiple scattering on the rainbow structure and the increased vertical depth in 3-D clouds.

The global cloud droplet radii results of POLDER in 2003 were compared with the MODIS estimates by Breon and Doutriaux-Boucher (2005). They showed that the POLDER- and MODIS-estimated CDRs are well correlated over the ocean, with a higher bias of approximately 2 µm for the MODIS results. The correlation breaks down over most land and polluted oceanic surfaces, where POLDER tends to estimate more small droplets (i.e., CDR less than 7 µm). The cause for the differences in the





AMTD
8, 6559–6597, 2015



CDR estimate from the two sensors remains unknown, although one hypothesis is the impact of cloud inhomogeneity in POLDER's retrieval. It should be noted that the spatial resolution of the POLDER CDR products (150 km) is much larger than that of the MODIS products (5 km). Further investigation is required to better understand the effects of cloud horizontal inhomogeneity on the polarized retrieval of cloud droplet sizes from POLDER.

As POLDER passes over a target, approximately 13 (up to 16) directional radiance measurements (for each spectral band) are acquired, and only limited measurements fall within the valid scattering angle region. The current POLDER CDR and EV retrieval algorithm employs measurements from $25 \times 25$ pixels to compensate for the insufficient angular sampling in the rainbow region. The measurements for the various pixels are acquired with different viewing geometries so that the combination of the observations provides near-continuous directional sampling of the polarization signature. However, this method relies on the assumption of homogeneity of the cloud over large distances (Breon and Doutriaux-Boucher, 2005; Bréon and Colzy, 2000). Actual clouds may not satisfy the homogeneity assumption (Schutgens and Roebeling, 2009). Moreover, the coarse resolution limits the usage in some aerosol-cloud interaction studies (Sekiguchi, 2003; Gryspeerdt et al., 2014). Based on the above analysis, the following two questions are the focal points of this study:

1. What are the effects of cloud horizontal inhomogeneity on the CDR and EV estimates from multi-angle polarized observations?

2. Can droplet size distributions be retrieved with reduced directional sampling from POLDER measurements, i.e., which would allow a better spatial resolution?

To answer these questions, both the POLDER-like data simulated with the RT3 model and the POLDER L1B measurements were used. The remainder of this paper is organized as follows. In Sect. 2, POLDER's polarized CDR and EV retrieval procedure is described. The retrieval cases, which are aimed at examining the effects of cloud horizontal inhomogeneity on the CDR, EV and COT, are presented in Sect. 3. Then,





AMTD
8, 6559–6597, 2015



the impact of directional sampling on the retrieval is presented, considering both the performances in different wavelengths and noise in the inversion. Sub-scale retrieval cases based on POLDER measurements are provided in Sect. 4, and the study is summarized in Sect. 5.

## 2 Data and methods

### 2.1 POLDER observations

POLDER is a sensor of the French space agency (CNES), which was launched on PARASOL in December 2004. It is a multi-spectral imaging polarimeter composed of a two-dimensional charged coupled device (CCD) detector array, a rotating wheel with spectral filters and polarizers, and a wide field-of-view (1800 km) telecentric optics (Parol et al., 2004; Tanre et al., 2011). The CCD detector array (242 × 274) provides a spatial resolution of approximately 6 km at nadir. When it passes over a target, the POLDER instrument acquires up to 16 successive multi-angle measurements of both the total and polarized reflected solar radiance in nine narrow channels with center wavelengths of 443, 490, 565, 670, 763, 765, 865, 910 and 1020 nm. For three of the eight spectral bands (490, 670 and 865 nm), a polarizer is added to the filters to assess the degree of linear polarization and the polarization direction, which are related to the $\boldsymbol{I}$, $\boldsymbol{Q}$, and $\boldsymbol{U}$ Stokes vectors of the polarization (Leroy et al., 1997). The second component of the vector $\boldsymbol{Q}$ is described with respect to the scattering plane defined by the solar and viewing directions.

In December 2009, PARASOL was maneuvered out of the Afternoon Constellation, known as the "A-Train" (Nakajima et al., 2010a; Stephens et al., 2002). The POLDER measurements before 2009 compare well with the other sensors (Stubenrauch et al., 2013; Zeng et al., 2011). Therefore, the POLDER L1B radiance and L2 CDR Products in 2008 were used in this study. The polarized reflectance $R_p$ adopted in this study was





AMTD
8, 6559–6597, 2015



normalized as follows:

$$R_p = -\frac{4Q}{\mu_s E_0}\left(1+\frac{\mu_v}{\mu_s}\right), \quad (1)$$

where $E_0$ ($W \cdot m^{-2}$) is the extraterrestrial solar irradiance, and $\mu_s$ and $\mu_v$ are the cosines of the solar and viewing zenith angles, respectively. The polarized reflectance is positive when the polarization direction is orthogonal to the scattering plane and negative when it is parallel to that plane. Note that most scattering and reflection processes generate a polarization perpendicular to the scattering plane, so that the definition of $R_p$ used here leads to positive values. This choice of sign was adopted by Breon and Doutriaux-Boucher (2005) and is opposite that proposed by Alexandrov et al. (2012). The normalization term in the parenthesis is used so that $R_p$ is, in the single scattering approximation, proportional to the polarized scattering phase function.

### 2.2 POLDER cloud droplet retrievals

The CDR and EV are retrieved at a spatial resolution of approximately 100 km × 100 km and are not part of the standard POLDER/Parasol cloud parameters. However, the CDR retrieval is very precise and accurate when the requirements for narrow size distributions and homogeneous distributions are met. Both daily and monthly CDR data are available from http://www.icare.univ-lille1.fr/drupal/parasol/overview_product.





AMTD
8, 6559–6597, 2015



## 2.3 Method

To express the size and the width of the cloud droplet distribution, the CDR ($r_{\text{eff}}$) and EV ($v_{\text{eff}}$) are defined as (Hansen and Travis, 1974)

$$r_{\text{eff}} = \int_{r_1}^{r_2} \pi r^3 n(r) \mathrm{d}r \Big/ \int_{r_1}^{r_2} \pi r^2 n(r) \mathrm{d}r, \tag{2}$$

$$v_{\text{eff}} = \int_{r_1}^{r_2} (r - r_{\text{eff}})^2 \pi r^2 n(r) \mathrm{d}r \Big/ r_{\text{eff}}^2 \int_{r_1}^{r_2} \pi r^2 n(r) \mathrm{d}r, \tag{3}$$

where $n(r)\mathrm{d}r$ is the number of particles per unit volume with radius between $r$ and $r + \mathrm{d}r$, and $r_1$ and $r_2$ are the smallest and largest particles in the size distribution, respectively. In this study, we assumed that spherical droplets obey the standard Gamma size distribution (Breon and Doutriaux-Boucher, 2005):

$$n(r) = C r^{(1-3v_{\text{eff}})/v_{\text{eff}}} e^{-r/r_{\text{eff}} v_{\text{eff}}}, \tag{4}$$

$$C = N (r_{\text{eff}} v_{\text{eff}})^{(2v_{\text{eff}}-1)/v_{\text{eff}}} / \Gamma[(1 - 2v_{\text{eff}})/v_{\text{eff}}], \tag{5}$$

where $\Gamma$ is the gamma function, and $N$ is the total number of particles per unit volume. Radiative transfer simulations show that single scattering contributes most to the POLDER-observed polarized reflectance, the contribution from multiple scattering to the polarized reflectance is negligible (Bréon and Goloub, 1998).

Figure 1 presents the polarized phase functions (the phase matrix elements $P_{12}$) for a set of standard Gamma droplet size distributions. The calculations were performed using Mie theory. Typically, the angular positions of the maxima and minima in the polarized scattering phase function are sensitive to the CDR, and the polarized reflectance local maxima and minima are sensitive to the EV. The angular distance between maxima decreases with an increase of the wavelength. For example, there are twice as many oscillations at 490 than at 865 nm.





AMTD
8, 6559–6597, 2015



The multi-angular polarized reflectance observed by POLDER provides a near-direct measurement of the polarized phase function, which makes it possible to retrieve the CDR and EV simultaneously. The modeled polarized reflectance were fitted with the polarized scattering phase function according to the following relationship:

$$R_p(\lambda) = a \cdot P_p(\Theta, r_{eff}, v_{eff}, \lambda) + b \cdot \cos^2(\Theta) + c, \quad (6)$$

where $\Theta$ is the scattering angle, and the empirical fitting parameters $a$, $b$ and $c$ represent the polarized contributions from multiple scattering, Rayleigh scattering, aerosol extinction, ground surface reflectance of thin clouds and effects caused by rotation to the scattering plane. The $\cos^2(\Theta)$ factor is used to account for the Rayleigh scattering contributions. Alexandrov et al. (2012) suggest to use a free parameter $\delta$ ($\pm 0.2^\circ$) in Eq. (6) to resolve the uncertainties caused by the angular shifts. We do not adopt the $\delta$ optimization procedure bacause the magnitude of these errors are much smaller than the angular size of the POLDER pixels (6 km $\approx 0.5^\circ$ at nadir).

We adopt similar procedures to those applied by Breon and Doutriaux-Boucher (2005), although some improvements were made:

1. While the original algorithm use the measurements in the range 145–180° of scattering angle, we also use those in the primary rainbow region (137–145°). These angles were used to increase the retrieval accuracy of large CDRs (15–20 µm). In addition, we added the polarized phase functions for EV = 0.1 in the LUT, allowing the EV to be retrieved over a broader range.

2. The $\cos^2(\Theta)$ term was used instead of $\Theta$ in the second term in Eq. (6) to match the POLDER measurements and the pre-computed phase functions because $\cos^2(\Theta)$ is more accurate for fitting (Alexandrov et al., 2012).

In the retrieval, the LUT of $P_{12}$ used is pre-calculated with an angular resolution of 0.5° for the rainbow scattering angles. The CDR values in LUT ranged from 5 to 20 µm with 0.5 µm increments, and the EV values included 0.01, 0.02, 0.05 and 0.1.





AMTD
8, 6559–6597, 2015



We first determine the $P_{12}$ values from the LUT based on the angular information of the observed polarized reflectances (OPRs); the $a$, $b$ and $c$ parameters are regressed using multiple linear regression fit, then many group modeled polarized reflectances (MPRs) are obtained according to Eq. (6). To evaluate the accuracy of the retrieval, two fit evaluations, i.e., $T_1$ and $T_2$, for the OPRs and MPRs were computed according to Eqs. (7) and (8)

$$T_1 = \text{correlate(OPRs,MPRs)}, \tag{7}$$

$$T_2 = \sqrt{\frac{\sum_{\text{SA}}(\text{OPRs-MPRs})^2}{N}}, \tag{8}$$

where $T_1$ and $T_2$ stand for the correlation coefficient and the root-mean-square error, respectively, of the measured and modeled reflectance arrays; $N$ represent the number of observations. The CDR and EV were derived from the MPRs according to the minimum $T_2$ and $T_1$ exceeding a predefining threshold.

## 3 Retrieval tests using RT3 simulations

The plane-parallel polarized radiative transfer (RT3) model was used to simulate POLDER-like reflectances from a cloud field with known droplet size distribution information (Wang et al., 2012). The RT3 model was developed for forward modeling of reflectances for plane-parallel atmospheres; it is the same as the vector radiative transfer model used by Hansen and Travis (1974) and Alexandrov et al. (2012). The contributions of both single scattering and multiple scattering are considered. The radiance exiting a vertically inhomogeneous atmosphere containing liquid cloud particles is computed with the doubling and adding method. Detailed information about the RT3 model are provided in Evans and Stephens (1991).

We analyzed various combinations of the CDR and EV at the POLDER polarized channels wavelengths (490, 670 and 865 nm). The CDR values ranged from 5 to 20 µm





AMTD
8, 6559–6597, 2015



with 1 µm increments, and the EV values were 0.01, 0.02 and 0.05. The atmosphere (Table 1) was assumed to consist of three plane-parallel layers (Cheng et al., 2008), and the Rayleigh optical thickness in different wavelength was set according to the results of Bodhaine et al. (1999). When the optical thickness of the cloud layer exceeds 5, the cloud polarization signal saturates, and the contributions from the underlying surface, aerosol and molecule layers are negligible (Coddington et al., 2010; Goloub et al., 2000). The solar zenith angle and the relative azimuth angle were assumed to be 20 and 180°, respectively. The sensor was assumed to be in the principal plane, which avoids potential error induced by the rotation to the scattering plane (Hansen and Travis, 1974; Alexandrov et al., 2012).

### 3.1 The sub-scale variability in the CDR and EV

The impact of the sub-scale variability in the CDR and EV is assessed through a model cloud field consisting of several equal-area sub-regions that share a constant COT but with variable CDR and EV values. Retrievals from a heterogeneous cloud field are presented in Fig. 2. The polarized reflectances were simulated at 865 nm. In Fig. 2a, we assumed that a third of a POLDER pixel was covered by a cloud with CDR = 10 and EV = 0.01, a third was covered by a cloud with CDR = 15 and EV = 0.01, and the other third was covered by a cloud with CDR = 20 and EV = 0.01. Similarly, In Fig. 2b, half of a POLDER pixel was assumed to be covered by a cloud with CDR = 10 and EV = 0.01, whereas the other half was covered by a cloud with CDR = 20 and EV = 0.01. The examples in Figs. 2a and b illustrate the retrieved CDR based on mean reflectance of inhomogeneous pixels tends to be bigger than the mean of the sub-pixel CDRs. Furthermore, the retrieved EV was greater than that at the sub-pixels, because the averaging of the signal from different CDR reduces the amplitude of the polarized reflectance oscillations. Figure 2c assume same CDRs but different EV values (0.01, 0.02 and 0.05) within three sub-pixels, the retrieved CDR is accurate and the retrieved EV is close to the mean of the sub-pixel EV values.





AMTD
8, 6559–6597, 2015



The scattering angle range used in the operational POLDER procedure is 145–165° and does not include the main rainbow region of 137–145°. To further assess the information content of the main rainbow structure for the retrieval, more cases were examined with respect to CDR variability. Each case was retrieved twice, either using the 137–165 or the 145–165° scattering angle ranges. The results shown in Table 2 demonstrate that the former is more stable than the latter. Indeed, the CDR estimates when using the 137–165° scattering angle range fall between the minimum and maximum CDRs, while the CDR estimates for the 145–165° range are often outside of the range of the simulated cloud. Regarding the EV estimates, the two retrievals resulted in no identifiable trends.

In conclusion, the heterogeneity in the cloud field CDR has a large impact on its mean estimate when using the polarization information. However, the impact of this variability is very much reduced when using information content of the primary rainbow (angular range 137–145°).

### 3.2 The sub-scale variability in COT

The current POLDER size distribution retrieval procedure adopts a relatively coarse resolution that may introduce errors by simply assuming that a cloud is homogeneous within an area of 150 km × 150 km. We considered a heterogeneous cloud with a constant CDR and variable optical depth to investigate whether the variability in the COT affects the POLDER retrievals. The polarized reflectance for heterogeneous cloud fields with COT = 1, 5, and 10 and CDR = 5, 11, and 16 µm were simulated using the RT3 model for the wavelength 865 nm. The size distribution retrieval results are presented in Table 3. The results indicate that, in most cases, the COT variability has a negligible impact on the CDR estimate, although it does affect the EV retrieved values. The variability in COT in a cloud field changes the amplitude of the rainbow structure, which is similar to the impact of the EV, while the angular positions of the peak values are insensitive to changes in the COT. Figure 3 illustrates the combination of COT = 1, 5, and 10 for CDR = 11 µm and EV = 0.02. All areas (different COT) generate a polarized





AMTD
8, 6559–6597, 2015



reflectance with a similar angular shape. The mixed curve agrees well with the best fit curve so that the retrieval is very accurate.

In conclusion, our simulations indicate that the spatial variability of the cloud optical thickness has no discernable impact on the CDR estimate when using the retrieval method based on the polarized reflectance. On the other hand, this variability does have some impact on the retrieval of the effective variance.

### 3.3 The number of observations used in the retrieval

To understand whether a resolution is sufficient for POLDER droplet size retrievals, the effects of directional sampling were investigated. As expected, assuming that the POLDER measurements are distributed with the same interval along the rainbow region, the lowest number of observations required for the retrievals directly determines the optimal resolution of POLDER's retrievals. By controlling the number of POLDER-like polarized reflectance observations ($N$) used in the retrieval, the relationship between the retrieval accuracy and the number of observations can be analyzed. Before the simulation, we compared the directional distribution of the scattering angle (SA) with real POLDER data and found that the measurements had nearly the same SA interval, ranging from 4 to 10°, which is determined by the solar-view geometry, time interval between successive acquisitions, and satellite speed. The satellite speed and period of acquisition are constant, but the solar zenith angle varies along the orbit, therefore the viewing geometry in the cloudbow view direction varies along the orbit. In the simulated cases described below, we assume that the POLDER multi-directional observations cover the entire cloudbow angular range and are evenly distributed. We also assumed that the measurements are not affected by noise induced by the instrument and the spatial structure of clouds. The number of observations modeled was no more than 32 for a certain pixel. Hence, we calculated the POLDER-like reflectances along the rainbow region with a 1° interval using cubic spline interpolation. In each retrieval test, the observations were evenly distributed over the rainbow scattering range (137–165°).





AMTD
8, 6559–6597, 2015



Comparisons of the retrievals at 865 nm with the actual CDR and EV values are shown in Fig. 4; $N$ was increased from 5 to 100 in these simulations. The results suggest that the correlation ($R^2$) and root-mean-square error (RMSE) does not change as $N$ exceeds12. Each plot contains 16 retrievals with the actual CDR ranging from 5 to 20 µm. As the number of observations was increased from 5 to 8, an increase in the $R^2$ between the CDR retrievals and the actual values was observed; the retrieval accuracy of the EV also improved for larger $N$. The $R^2$ and the RMSE for $N > 12$ are stable at 0.99 and 0.13, respectively.

As expected, the error in the CDR and EV retrievals was larger for small $N$ (less than 8), indicating that the observed rainbow structure curve requires more observations. The observed rainbow structure and the best fit curves for two cases when $N = 5$ are plotted in Fig. 5a and b, although the result is invalid despite the good accuracies. Moreover, Fig. 5c and d presents reliable fitting curves when $N = 12$. The observed rainbow structure and the best fit curves do not perfectly coincide with each other; uncertainties are induced by the spline interpolation. These results confirm that the observed rainbow structures can be precisely represented when sufficient observations are provided.

### 3.4 *N* requirements at different wavelengths

Because the oscillations in the rainbow structure vary with wavelength, the number of observations required at different wavelengths also differs. We applied the retrieval for various CDR and EV values at wavelengths of 490, 670 and 865 nm independently. To compare the results in these three wavelengths, the RMSE between the 16 group retrievals (the actual CDRs ranged from 5 to 20 µm) were derived for EV = 0.01, 0.02 and 0.05 and at wavelengths of 670 and 865 nm, respectively. At 490 nm, the RMSE were derived from 11 group retrievals (the actual CDRs ranged from 5 to 15 µm) for three EV values because the Legendre series for cloud fields with effective radii greater than 15 µm exceeded the limitations of the RT3 model.





AMTD
8, 6559–6597, 2015



Figure 6a–c presents RMSE comparison results at three wavelengths for a cloud field with EVs of 0.01, 0.02 and 0.05, respectively. The performance for 490 nm is better than 670 nm is attributable to the absence of the large droplets (> 15 µm) in comparison. When the large droplets are removed from the comparison, the performances in three wavelengths are samely good. At least 11observations are needed for the 670 nm wavelength to keep RMSE less than 1; however, the number of observations needed at 865 nm is 8. This difference is because the increase in wavelength led to more oscillations, which require more observations to fit the curve. As EV increased, the slopes of the oscillations became gentler, which is why fewer observations were required. For limited observations, wavelengths of 865 or 670 nm instead of 490 nm for retrievals were found to be more reliable, especially for large droplets. The EV retrieval accuracies for the three wavelengths share a similar trend with the CDR retrievals: fewer observations were required at larger wavelengths. A comparison of the retrievals for the three wavelengths using 12 observations with the actual EV = 0.02 is presented in Table 4.

In conclusion, the accuracy of the retrieval results increases with an increase of the wavelength. Thus, for POLDER, the 865 nm channel is better suited than the other two channels. However, the shorter wavelength channel do bring additional information and may be used together with the 865 nm for a better constrain on the cloud parameters.

### 3.5 Noise in the retrievals

The theoretical analysis in Sects. 3.1 and 3.2 indicate that the inversion is rather stable if a sufficient number of observations is provided. However, the POLDER observations are not always optimal; noise may be introduced from instruments, the transmission of the signal and the inhomogeneous structure of cloud fields. Such noise can be taken as pseudo-random errors added on the multi-angle polarized reflectances (Fougnie et al., 2007; Cairns et al., 2003).

To analyze the sensitivity of the droplet size retrieval to the noise, we add Gaussian noise with increasing standard deviation to simulated polarized reflectances (van





AMTD
8, 6559–6597, 2015



Diedenhoven et al., 2012). Retrievals at 865 nm with actual CDR values of 5–20 µm and actual EV of 0.05 are evaluated. Considering the influence of Gaussian noise is related to the number of observations, we applied each retrieval three times, either with 9, 12 and 20 observations in the rainbow region. As shown in Fig. 7, the retrievals are essentially unaffected by random noise when the standard deviations less than 10 % of the signal. The RMSE values and the maximum errors (not shown) in CDR estimation is no more than 0.05 and 1 µm, respectively. For noise contributions larger than the 10 % of the signal, the RMSE values of CDR estimation quickly increase. The noise generated from the instrument and calibration in POLDER measured polarized reflectance are considered within 3 % (van Diedenhoven et al., 2012; Fougnie et al., 2007). These results confirm that the inversion is robust as long as the noise contributions does not exceed 10 % of the valid signal, even if the observations are limited.

## 4 POLDER retrieval results

### 4.1 Comparisons with the official CDRs

We applied the size distribution retrievals to the improved method using the global POLDER L1B data from June 2008. The retrievals were performed for scattering angles of 137–165°; the polarized reflectances at 865 nm wavelength were used and the resolution applied was 150 km × 150 km. To make the comparison more convenient and reliable, the inversion was performed according to the geolocations of official size distribution products. We add the inversion quality index (Qual) that has been adopted by the operational procedure. Qual is based on the ratio between the variability of the signal and the RMS error of the fit, detail information of Qual can be found in (Breon and Doutriaux-Boucher, 2005). Strict conditions ($T_1 > 0.98$ and Qual > 6) were used to select the new retrievals, and the comparisons with the official CDRs are shown in Fig. 8. The CDRs derived from the improved method are well correlated with the official CDRs of 5 to 14 µm. However, for CDRs of 15 to 19 µm newly derived, large





AMTD
8, 6559–6597, 2015



differences between the two approaches are found with an official estimation low bias of about 2–4 µm.

The bias of CDRs (> 15 µm) between the two approaches can be explained by the absence of measurements from the primary rainbow region (137–145°) in the official retrieval procedure. According to Fig. 1a, the cloudbow oscillations (137–145°) for CDR > 15 µm were more pronounced than for smaller CDRs (< 15 µm), and the cloudbow oscillations (145–165°) attenuated faster for larger CDRs. For example, the cloudbow oscillations for CDR = 19 µm were very weak for scattering angles exceeding 155°, although intense oscillations were found from the cloudbow for CDR = 5 µm, even at a scattering angle of 170°. Table 5 presents comparisons between CDRs estimated using POLDER-like measurements for the 137–165 and 145–165° scattering angle ranges. The retrievals for CDR < 15 µm were accurate in both groups. The CDRs derived from 145–165 scattering angle range tend to be underestimated. While in the 137–165° range, the retrievals were more reliable across the entire CDR range. There are other reasons that may explain the difference between our results and the POLDER data, including the criteria used for selecting best fit results and the number of wavelengths employed in the retrievals. However, we do not believe these differences can introduce large biases because we added the Qual factor in the retrieval to preserve the accuracy of our results. Although wavelengths of 490, 679 and 865 nm are used in POLDER's retrieval algorithm, the cases presented in Sect. 3.4 demonstrate that the retrieval is robust when applied at 865 nm.

### 4.2 Sub-scale retrievals

The aforementioned analysis revealed that the proposed algorithm is robust when sufficient observations are obtained in the rainbow region and that the heterogeneity of clouds can leaded to biased estimates of the CDR and EV distributions. It is necessary to examine the operational retrievals at a higher resolution and compare the results with the official products.





AMTD
8, 6559–6597, 2015



A case study was conducted with a resolution of 7 × 7 pixels for the data from 1 June 2008. We divided the grid (150 km × 150 km) into 36 sub-grids to derive derailed CDR information at the sub-grid scale. In accordance with previous analyses, retrievals can be conducted with approximately 10 observations at scattering angles of 137–165° in 865 nm wavelength. Considering instrumental noise, we applied the retrieval to observations that encompassed the entire rainbow region; the number of polarized reflectances exceeded 15. The grid and sub-grid retrievals at 70.5° W, 172.1° N are shown in Fig. 9a and b. In the official CDR products, the grid-scale CDR and EV were 10.5 µm and 0.05, respectively. The same CDR was retrieved using our algorithm, although our EV was 0.1. The EV difference was caused by the polarized phase functions for EV = 0.1 not being included in the operational procedure. According to the sub-scale retrievals shown in Fig. 9b, 24 effective grid-scale retrievals were derived with CDRs ranging from 6 to 14.5 µm. The sub-scale average of the CDRs was 9.92 µm, which was less than the grid-scale retrieval result. However, we emphasize that the results presented herein are based on a particular case that is not representative of all POLDER observations. The impact of drizzle in this region is unclear and must be elucidated in future research.

## 5 Conclusions

In this study, Our retrieval algorithm is based on the ideas of (Bréon and Goloub) or (Bréon and Doutriaux-Boucher) but with significant improvements concerning the use of measurements in the primary rainbow region (137–145°) to provide more reliable large droplet (> 15 µm) retrievals. Multi-angular POLDER-like polarized reflectances at wavelengths of 490, 670 and 865 nm from cloud fields with known droplet size distributions and optical thicknesses were simulated using the RT3 model and Mie theory. These simulated observations were used to analyze the impacts of cloud horizontal inhomogeneity and directional sampling on the retrievals. The sub-scale variability of the CDR distributions induces uncertainties in the CDR and EV retrievals because the ob-





AMTD
8, 6559–6597, 2015



served rainbow structure was determined by the proportions of sub-parts with different DERs. However, the sub-scale variability in the EV and COT affects the EV retrievals, but with discernable impact on the CDR estimates. Therefore, Higher-resolution retrievals should be applied in order to reduce the biases introduced by the effects of cloud horizontal inhomogeneity.

To understand whether a resolution is sufficient for POLDER droplet size retrievals, the effects of directional sampling were investigated. Case studies showed that the algorithm is robust when sufficient measurements are provided, and the required number of measurements was found to decrease as the wavelength increased from 490 to 865 nm, which is determined by the cloudbow oscillations at those wavelengths. Furthermore, the retrieval is robust as long as the random noise is no more than the 10 % of the signal.

The POLDER global L1B data for June 2008 were used to derive the CDRs using the improved method and for comparison with the official CDR products. The CDRs derived using the improved method are well correlated with the official products for CDRs of 5 to 14 µm; however, for CDRs of 15 to 19 µm, the official CDRs were underestimated by 2–4 µm. The cases using the POLDER-like measurements had similar results. These biases can be explained by the absence of measurements from the primary rainbow region (137–145°), where the cloudbow oscillations for large droplets are more pronounced than for smaller droplets (CDR < 15 µm). Finally, a case study illustrated that the cloud size distribution retrievals can be performed at 7 × 7 pixels. The results suggest that the POLDER size distribution retrieval algorithm can be applied at a higher resolution and that substantial uncertainties due to cloud horizontal inhomogeneity exist.

Several questions require further investigation. For example, if the cloud size distribution is inferred at a higher resolution, will the bias between the MODIS and POLDER CDRs still exist? A long series of POLDER CDRs should be derived with a higher resolution, and the results should be compared with the POLDER and MODIS CDR





AMTD
8, 6559–6597, 2015



products. In addition, the theoretical minimum number of measurements needed for cloud size distribution retrievals can help guide instrument design and improvement.

*Acknowledgements.* This work was supported in part by the CAS/SAFEA International Partnership Program for Creative Research Teams under Grant KZZD-EW-TZ-09. The Data used in this paper were derived from the CNES/POLDER instrument onboard NASDA/ADEOS. The authors thank the Interactions Clouds Aerosols Radiations Etc (ICARE) thematic center for processing the POLDER data. We are grateful to K. F. Evans at University of Colorado for the Radiative Transfer 3 and Mie codes.

## References

Alexandrov, M. D., Cairns, B., Emde, C., Ackerman, A. S., and van Diedenhoven, B.: Accuracy assessments of cloud droplet size retrievals from polarized reflectance measurements by the research scanning polarimeter, Remote Sens. Environ., 125, 92–111, doi:10.1016/j.rse.2012.07.012, 2012.

Baum, B. A., Kratz, D. P., Yang, P., Ou, S. C., Hu, Y. X., Soulen, P. F., and Tsay, S. C.: Remote sensing of cloud properties using MODIS airborne simulator imagery during SUCCESS 1. Data and models, J. Geophys. Res.-Atmos., 105, 11767–11780, doi:10.1029/1999jd901089, 2000.

Bodhaine, B. A., Wood, N. B., Dutton, E. G., and Slusser, J. R.: On Rayleigh optical depth calculations, J. Atmos. Ocean. Tech., 16, 1854–1861, doi:10.1175/1520-0426(1999)016<1854:orodc>2.0.co;2, 1999.

Bréon, F.-M. and Colzy, S.: Global distribution of cloud droplet effective radius from POLDER polarization measurements, Geophys. Res. Lett., 27, 4065–4068, doi:10.1029/2000gl011691, 2000.

Breon, F. M. and Doutriaux-Boucher, M.: A comparison of cloud droplet radii measured from space, IEEE T. Geosci. Remote, 43, 1796–1805, doi:10.1109/TGRS.2005.852838, 2005.

Bréon, F.-M. and Goloub, P.: Cloud droplet effective radius from spaceborne polarization measurements, Geophys. Res. Lett., 25, 1879–1882, doi:10.1029/98gl01221, 1998.

Cairns, B., Russell, E. E., LaVeigne, J. D., and Tennant, P. M. W.: Research scanning polarimeter and airborne usage for remote sensing of aerosols, in: Polarization Science and Remote





AMTD
8, 6559–6597, 2015



Sensing, edited by: Shaw, J. A. and Tyo, J. S., Proceedings of SPIE – The International Society for Optical Engineering, 33–44, 2003.
Cheng, T. H., Gu, X. F., Chen, L. F., Yu, T., and Tian, G. L.: Multi-angular polarized characteristics of cirrus clouds, Acta Phys. Sin., 57, 5323–5332, 2008.
Coddington, O. M., Pilewskie, P., Redemann, J., Platnick, S., Russell, P. B., Schmidt, K. S., Gore, W. J., Livingston, J., Wind, G., and Vukicevic, T.: Examining the impact of overlying aerosols on the retrieval of cloud optical properties from passive remote sensing, J. Geophys. Res., 115, D10211, doi:10.1029/2009jd012829, 2010.
Dandin, P., Pontikis, C., and Hicks, E.: Sensitivity of a GCM to changes in the droplet effective radius parameterization, Geophys. Res. Lett., 24, 437–440, doi:10.1029/97gl00214, 1997.
Di Girolamo, L., Liang, L., and Platnick, S.: A global view of one-dimensional solar radiative transfer through oceanic water clouds, Geophys. Res. Lett., 37, L18809, doi:10.1029/2010gl044094, 2010.
Evans, K. F. and Stephens, G. L.: A new polarized atmospheric radiative-transfer model, J. Quant. Spectrosc. Ra., 46, 413–423, doi:10.1016/0022-4073(91)90043-p, 1991.
Fougnie, B., Bracco, G., Lafrance, B., Ruffel, C., Hagolle, O., and Tinell, C.: PARASOL in-flight calibration and performance, Appl. Optics, 46, 5435–5451, doi:10.1364/ao.46.005435, 2007.
Goloub, P., Herman, M., Chepfer, H., Riedi, J., Brogniez, G., Couvert, P., and Séze, G.: Cloud thermodynamical phase classification from the POLDER spaceborne instrument, J. Geophys. Res., 105, 14747, doi:10.1029/1999jd901183, 2000.
Gryspeerdt, E., Stier, P., and Partridge, D. G.: Satellite observations of cloud regime development: the role of aerosol processes, Atmos. Chem. Phys., 14, 1141–1158, doi:10.5194/acp-14-1141-2014, 2014.
Hansen, J. and Travis, L.: Light scattering in planetary atmospheres, Space Sci. Rev., 16, 527–610, doi:10.1007/BF00168069, 1974.
Haywood, J. M., Osborne, S. R., and Abel, S. J.: The effect of overlying absorbing aerosol layers on remote sensing retrievals of cloud effective radius and cloud optical depth, Q. J. Roy. Meteor. Soc., 130, 779–800, doi:10.1256/qj.03.100, 2004.
Horváth, Á.: Anisotropy of water cloud reflectance: a comparison of measurements and 1-D theory, Geophys. Res. Lett., 31, L01102, doi:10.1029/2003gl018386, 2004.
Kawamoto, K., Nakajima, T., and Nakajima, T. Y.: A global determination of cloud microphysics with AVHRR remote sensing, J. Climate, 14, 2054–2068, doi:10.1175/1520-0442(2001)014<2054:agdocm>2.0.co;2, 2001.





AMTD
8, 6559–6597, 2015



Leroy, M., Deuzé, J. L., Bréon, F. M., Hautecoeur, O., Herman, M., Buriez, J. C., Tanré, D., Bouffiès, S., Chazette, P., and Roujean, J. L.: Retrieval of atmospheric properties and surface bidirectional reflectances over land from POLDER/ADEOS, J. Geophys. Res., 102, 17023, doi:10.1029/96jd02662, 1997.

Liu, Y. G., Daum, P. H., and Hallett, J.: A generalized systems theory for the effect of varying fluctuations on cloud droplet size distributions, J. Atmos. Sci., 59, 2279–2290, doi:10.1175/1520-0469(2002)059<2279:agstft>2.0.co;2, 2002.

Liu, Y., Wu, W., Jensen, M. P., and Toto, T.: Relationship between cloud radiative forcing, cloud fraction and cloud albedo, and new surface-based approach for determining cloud albedo, Atmos. Chem. Phys., 11, 7155–7170, doi:10.5194/acp-11-7155-2011, 2011.

Marshak, A., Platnick, S., Várnai, T., Wen, G., and Cahalan, R. F.: Impact of three-dimensional radiative effects on satellite retrievals of cloud droplet sizes, J. Geophys. Res., 111, D09207, doi:10.1029/2005jd006686, 2006.

Nagao, T. M., Suzuki, K., and Nakajima, T. Y.: Interpretation of multiwavelength-retrieved droplet effective radii for warm water clouds in terms of in-cloud vertical inhomogeneity by using a spectral bin microphysics cloud model, J. Atmos. Sci., 70, 2376–2392, doi:10.1175/jas-d-12-0225.1, 2013.

Nakajima, T. and King, M. D.: Determination of the optical-thickness and effective particle radius of clouds from reflected solar-radiation measurements, J. Atmos. Sci., 47, 1878–1893, doi:10.1175/1520-0469(1990)047<1878:dotota>2.0.co;2, 1990.

Nakajima, T. Y. and Nakajima, T.: Wide-area determination of cloud microphysical properties from NOAA AVHRR measurements for FIRE and ASTEX regions, J. Atmos. Sci., 52, 4043–4059, doi:10.1175/1520-0469(1995)052<4043:wadocm>2.0.co;2, 1995.

Nakajima, T. Y., Suzuki, K., and Stephens, G. L.: Droplet growth in warm water clouds observed by the a-train, Part II: a multisensor view, J. Atmos. Sci., 67, 1897–1907, doi:10.1175/2010jas3276.1, 2010a.

Nakajima, T. Y., Suzuki, K., and Stephens, G. L.: Droplet growth in warm water clouds observed by the a-train, Part I: Sensitivity analysis of the MODIS-derived cloud droplet sizes, J. Atmos. Sci., 67, 1884–1896, doi:10.1175/2009jas3280.1, 2010b.

Parol, F., Buriez, J. C., Vanbauce, C., Riedi, J., C.-Labonnote, L., Doutriaux-Boucher, M., Vesperini, M., Sèze, G., Couvert, P., Viollier, M., and Bréon, F. M.: Review of capabilities of multi-angle and polarization cloud measurements from POLDER, Adv. Space Res., 33, 1080–1088, doi:10.1016/s0273-1177(03)00734-8, 2004.





AMTD
8, 6559–6597, 2015



Penner, J. E., Dong, X. Q., and Chen, Y.: Observational evidence of a change in radiative forcing due to the indirect aerosol effect, Nature, 427, 231–234, doi:10.1038/nature02234, 2004.
Platnick, S., King, M. D., Ackerman, S. A., Menzel, W. P., Baum, B. A., Riedi, J. C., and Frey, R. A.: The MODIS cloud products: algorithms and examples from Terra, IEEE T. Geosci. Remote, 41, 459–473, doi:10.1109/TGRS.2002.808301, 2003.
Sayer, A. M., Poulsen, C. A., Arnold, C., Campmany, E., Dean, S., Ewen, G. B. L., Grainger, R. G., Lawrence, B. N., Siddans, R., Thomas, G. E., and Watts, P. D.: Global retrieval of ATSR cloud parameters and evaluation (GRAPE): dataset assessment, Atmos. Chem. Phys., 11, 3913–3936, doi:10.5194/acp-11-3913-2011, 2011.
Schutgens, N. A. J. and Roebeling, R. A.: Validating the validation: the influence of liquid water distribution in clouds on the intercomparison of satellite and surface observations, J. Atmos. Ocean. Tech., 26, 1457–1474, doi:10.1175/2009jtecha1226.1, 2009.
Sekiguchi, M.: A study of the direct and indirect effects of aerosols using global satellite data sets of aerosol and cloud parameters, J. Geophys. Res., 108, 4699, doi:10.1029/2002jd003359, 2003.
Shang, H., Chen, L., Tao, J., Su, L., and Jia, S.: Synergetic use of MODIS cloud parameters for distinguishing high aerosol loadings from clouds over the North China Plain, IEEE J. Sel. Top. Appl., 7, 4879–4886, doi:10.1109/jstars.2014.2332427, 2014.
Stephens, G. L., Vane, D. G., Boain, R. J., Mace, G. G., Sassen, K., Wang, Z., Illingworth, A. J., O'Connor, E. J., Rossow, W. B., Durden, S. L., Miller, S. D., Austin, R. T., Benedetti, A., Mitrescu, C., and CloudSat Science Team, T.: The Cloudsat Mission and the a-train, B. Am. Meteorol. Soc., 83, 1771–1790, doi:10.1175/bams-83-12-1771, 2002.
Stubenrauch, C. J., Rossow, W. B., Kinne, S., Ackerman, S., Cesana, G., Chepfer, H., Di Girolamo, L., Getzewich, B., Guignard, A., Heidinger, A., Maddux, B. C., Menzel, W. P., Minnis, P., Pearl, C., Platnick, S., Poulsen, C., Riedi, J., Sun-Mack, S., Walther, A., Winker, D., Zeng, S., and Zhao, G.: Assessment of global cloud datasets from satellites: project and database initiated by the GEWEX Radiation Panel, B. Am. Meteorol. Soc., 94, 1031–1049, doi:10.1175/bams-d-12-00117.1, 2013.
Tanré, D., Bréon, F. M., Deuzé, J. L., Dubovik, O., Ducos, F., François, P., Goloub, P., Herman, M., Lifermann, A., and Waquet, F.: Remote sensing of aerosols by using polarized, directional and spectral measurements within the A-Train: the PARASOL mission, Atmos. Meas. Tech., 4, 1383–1395, doi:10.5194/amt-4-1383-2011, 2011.





AMTD
8, 6559–6597, 2015



van Diedenhoven, B., Cairns, B., Geogdzhayev, I. V., Fridlind, A. M., Ackerman, A. S., Yang, P., and Baum, B. A.: Remote sensing of ice crystal asymmetry parameter using multi-directional polarization measurements – Part 1: Methodology and evaluation with simulated measurements, Atmos. Meas. Tech., 5, 2361–2374, doi:10.5194/amt-5-2361-2012, 2012.

Vant-Hull, B., Marshak, A., Remer, L. A., and Zhanqing, L.: The effects of scattering angle and cumulus cloud geometry on satellite retrievals of cloud droplet effective radius, IEEE T. Geosci. Remote, 45, 1039–1045, doi:10.1109/TGRS.2006.890416, 2007.

Walther, A. and Heidinger, A. K.: Implementation of the daytime cloud optical and microphysical properties algorithm (DCOMP) in PATMOS-x, J. Appl. Meteorol. Clim., 51, 1371–1390, doi:10.1175/jamc-d-11-0108.1, 2012.

Walther, A., Heidinger, A. K., and Miller, S.: The expected performance of cloud optical and microphysical properties derived from Suomi NPP VIIRS day/night band lunar reflectance, J. Geophys. Res.-Atmos., 118, 13230–13240, doi:10.1002/2013jd020478, 2013.

Wang, Z., Chen, L., Li, Q., Li, S., Jiang, Z., and Wang, Z.: Retrieval of aerosol size distribution from multi-angle polarized measurements assisted by intensity measurements over East China, Remote Sens. Environ., 124, 679–688, doi:10.1016/j.rse.2012.06.021, 2012.

Wolters, E. L. A., Deneke, H. M., van den Hurk, B. J. J. M., Meirink, J. F., and Roebeling, R. A.: Broken and inhomogeneous cloud impact on satellite cloud particle effective radius and cloud-phase retrievals, J. Geophys. Res., 115, D10214, doi:10.1029/2009jd012205, 2010.

Zeng, S., Parol, F., Riedi, J., Cornet, C., and Thieuleux, F.: Examination of POLDER/PARASOL and MODIS/Aqua cloud fractions and properties representativeness, J. Climate, 24, 4435–4450, doi:10.1175/2011jcli3857.1, 2011.

Zhang, Z.: On the sensitivity of cloud effective radius retrieval based on spectral method to bi-modal droplet size distribution: a semi-analytical model, J. Quant. Spectrosc. Ra., 129, 79–88, doi:10.1016/j.jqsrt.2013.05.033, 2013.

Zhang, Z., Ackerman, A. S., Feingold, G., Platnick, S., Pincus, R., and Xue, H.: Effects of cloud horizontal inhomogeneity and drizzle on remote sensing of cloud droplet effective radius: case studies based on large-eddy simulations, J. Geophys. Res.-Atmos., 117, D19208, doi:10.1029/2012jd017655, 2012.

Zinner, T., Wind, G., Platnick, S., and Ackerman, A. S.: Testing remote sensing on artificial observations: impact of drizzle and 3-D cloud structure on effective radius retrievals, Atmos. Chem. Phys., 10, 9535–9549, doi:10.5194/acp-10-9535-2010, 2010.





AMTD
8, 6559–6597, 2015



**Table 1.** The atmospheric layers and components assumed in the RT3 model for simulating the POLDER-like polarized signal.

| Layers | Components | Properties |
|---|---|---|
| Surface | Ocean | Albedo = 0.02 |
| 0–3 km | Molecules, aerosols | $\tau_{molecular}$ = 0.051, 0.014 and 0.051 for 490, 670 and 865 nm wavelengths, respectively |
| | | $\tau_{aerosol}$ = 0.3 |
| 3 ~ 3.5 km | Liquid water clouds | $\tau_{clouds}$ = 1, 5, 10 |
| 3.5–15 km | Molecules | $\tau_{molecular}$ = 0.105, 0.029 and 0.104 for 490, 670 and 865 nm wavelengths, respectively |





AMTD
8, 6559–6597, 2015



**Table 2.** Retrievals from a heterogeneous cloud field with variable CDR using POLDER-like polarized reflectances in 137–165 and 145–165° ranges, respectively. In all cases, the EV in the sub-scale cloud and the COT were assumed to be 0.01 and 5, respectively. The "+" indicates the equal share of the CDRs in the cloud fields.

| | | Retrievals of 137–165° | | Retrievals of 145–165° | |
|---|---|---|---|---|---|
| Combined CDRs (μm) | EV | CDR (μm) | EV | CDR (μm) | EV |
| 5 + 10 | 0.01 | 8 | 0.1 | 19 | 0.02 |
| 5 + 15 | 0.01 | 14.5 | 0.01 | 10.5 | 0.1 |
| 5 + 20 | 0.01 | 19 | 0.01 | 6 | 0.1 |
| 10 + 15 | 0.01 | 13 | 0.05 | 18.5 | 0.01 |
| 10 + 20 | 0.01 | 16.5 | 0.1 | 14.5 | 0.02 |
| 15 + 20 | 0.01 | 18 | 0.01 | 10 | 0.02 |
| 5 + 10 + 15 | 0.01 | 12 | 0.1 | 19 | 0.1 |
| 5 + 10 + 20 | 0.01 | 14 | 0.1 | 19 | 0.02 |
| 5 + 15 + 20 | 0.01 | 17.5 | 0.02 | 11 | 0.1 |
| 10 + 15 + 20 | 0.01 | 16 | 0.1 | 8 | 0.01 |





AMTD
8, 6559–6597, 2015



**Table 3.** Retrievals from a heterogeneous cloud field with variable COT using POLDER-like polarized reflectances in 137–165° range. In all cases, the EV in the sub-scale cloud were assumed to be 0.02, and the CDR values included 5, 11 and 16 µm. The "+" indicates the equal share of the COTs in the cloud fields.

| Input Cloud Optical Thickness | Actual CDR (µm) | Actual EV | Retrieved CDR (µm) | Retrieved EV |
|---|---|---|---|---|
| 1 + 5 | 5 | 0.02 | 5 | 0.05 |
| 5 + 10 | 5 | 0.02 | 5 | 0.05 |
| 1 + 10 | 5 | 0.02 | 5 | 0.05 |
| 1 + 5 + 10 | 5 | 0.02 | 5 | 0.05 |
| 1 + 5 | 11 | 0.02 | 11 | 0.02 |
| 5 + 10 | 11 | 0.02 | 11 | 0.02 |
| 1 + 10 | 11 | 0.02 | 11 | 0.02 |
| 1 + 5 + 10 | 11 | 0.02 | 11 | 0.02 |
| 1 + 5 | 16 | 0.02 | 16 | 0.02 |
| 5 + 10 | 16 | 0.02 | 16 | 0.02 |
| 1 + 10 | 16 | 0.02 | 16 | 0.02 |
| 1 + 5 + 10 | 16 | 0.02 | 16 | 0.02 |





AMTD
8, 6559–6597, 2015



**Table 4.** Comparison of the CDR and EV retrievals for three wavelengths using 12 observations with the actual EV = 0.02; the COT was assumed to be 5 in all cases. The absence of retrievals for CDR = 16 ~ 20 μm is due to the Legendre series for cloud fields with effective radii greater than 15 μm that exceeds the limitations of the RT3 model.

| | 490 nm | | 670 nm | | 865 nm | |
|---|---|---|---|---|---|---|
| Actual CDR (μm) | CDR (μm) | EV | CDR (μm) | EV | CDR (μm) | EV EV |
| 5 | 5 | 0.02 | 5.5 | 0.02 | 5 | 0.05 |
| 6 | 6 | 0.02 | 6 | 0.01 | 6 | 0.02 |
| 7 | 7 | 0.02 | 7 | 0.01 | 7 | 0.02 |
| 8 | 8 | 0.02 | 8.5 | 0.02 | 8 | 0.02 |
| 9 | 9 | 0.02 | 9 | 0.01 | 9 | 0.02 |
| 10 | 10 | 0.05 | 10 | 0.02 | 10 | 0.02 |
| 11 | 11 | 0.05 | 11.5 | 0.02 | 11 | 0.02 |
| 12 | 12 | 0.05 | 12.5 | 0.02 | 12 | 0.02 |
| 13 | 13 | 0.05 | 14 | 0.05 | 13 | 0.02 |
| 14 | 14 | 0.05 | 15 | 0.05 | 14 | 0.02 |
| 15 | 15 | 0.05 | 16 | 0.02 | 15 | 0.02 |
| 16 | | | 16.5 | 0.02 | 15.5 | 0.02 |
| 17 | | | 19 | 0.05 | 17 | 0.05 |
| 18 | | | 19.5 | 0.05 | 18 | 0.05 |
| 19 | | | 20 | 0.05 | 19.5 | 0.2 |
| 20 | | | 20 | 0.05 | 20 | 0.02 |





AMTD
8, 6559–6597, 2015



**Table 5.** Comparisons between CDRs estimated using POLDER-like measurements for scattering angle ranges of 137–165 and 145–165°, respectively. The retrievals were applied using 40 measurements at a wavelength of 865 nm. The actual EV used include 0.01, 0.02 and 0.05.

| | CDRs retrieved for angles of 137–165° (μm) | | | CDRs retrieved for angles of 145–165° (μm) | | |
|---|---|---|---|---|---|---|
| CDR (μm) | 0.01 | 0.02 | 0.05 | 0.01 | 0.02 | 0.05 |
| 5 | 5 | 5 | 5 | 5 | 5 | 5 |
| 6 | 6 | 6 | 6 | 6 | 6 | 6 |
| 7 | 7 | 7 | 7 | 7 | 7 | 7 |
| 8 | 8 | 8 | 8 | 8 | 8 | 8 |
| 9 | 9 | 9 | 9 | 9 | 9 | 9 |
| 10 | 10 | 10 | 10 | 10 | 10 | 10 |
| 11 | 11 | 11 | 11 | 11 | 11 | 11 |
| 12 | 12 | 12 | 12 | 12 | 12 | 12 |
| 13 | 12.5 | 13 | 13 | 12.5 | 13 | 13 |
| 14 | 14 | 14 | 14 | 14 | 14 | 13.5 |
| 15 | 15 | 15 | 15 | 15 | 15 | 14.5 |
| 16 | 15.5 | 15.5 | 16 | 15.5 | 15 | 15 |
| 17 | 16 | 16 | 17 | 15.5 | 15.5 | 9.5 |
| 18 | 17 | 18 | 18 | 10.5 | 10.5 | 10 |
| 19 | 19 | 19 | 19 | 11 | 11.5 | 11 |
| 20 | 20 | 20 | 19.5 | 20 | 12 | 11.5 |





AMTD
8, 6559–6597, 2015



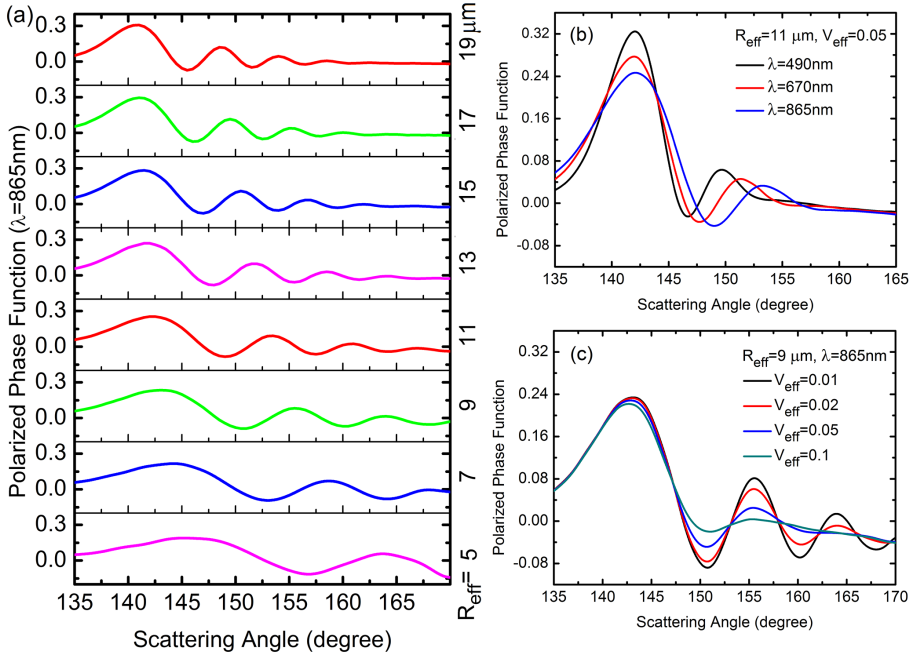


**Figure 1.** Simulations of polarized phase function ($P_p$) for various droplet effective radii, effective variances, and wavelengths. The left plot shows how $P_p$ varies with the effective radius; bottom right plot shows $P_p$ for various EV, while upper right plot shows the same for 3 wavelengths.





AMTD
8, 6559–6597, 2015

A better understanding of POLDER's cloud droplet size retrieval

H. Shang et al.



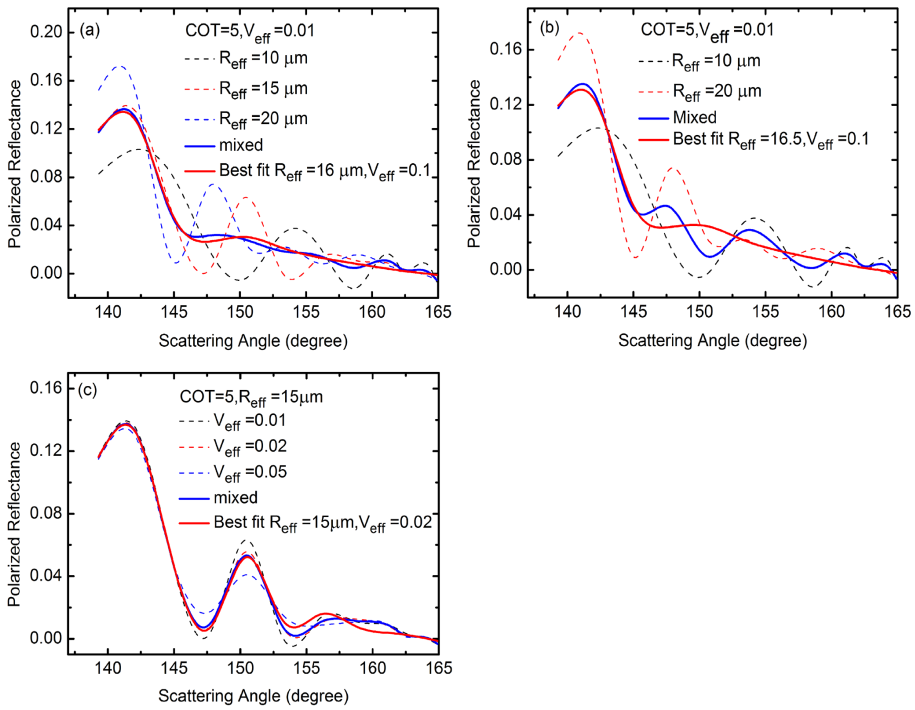


**Figure 2.** The retrievals from a heterogeneous cloud field with constant COT = 5 and variable CDR and EV values. The dashed lines indicate the separate rainbow structures for sub-scale cloud fields. Three equal-area sub-parts with CDR = 10, 15 and 20 μm were considered in **(a)**; two equal-area sub-parts with CDR = 10 and 20 μm were considered in **(b)**; three equal-area sub-parts with EV = 0.01, 0.02 and 0.05 were considered in **(c)**; the blue line represents the rainbow structure for the heterogeneous cloud field; the red line depicts the best fit.





AMTD
8, 6559–6597, 2015



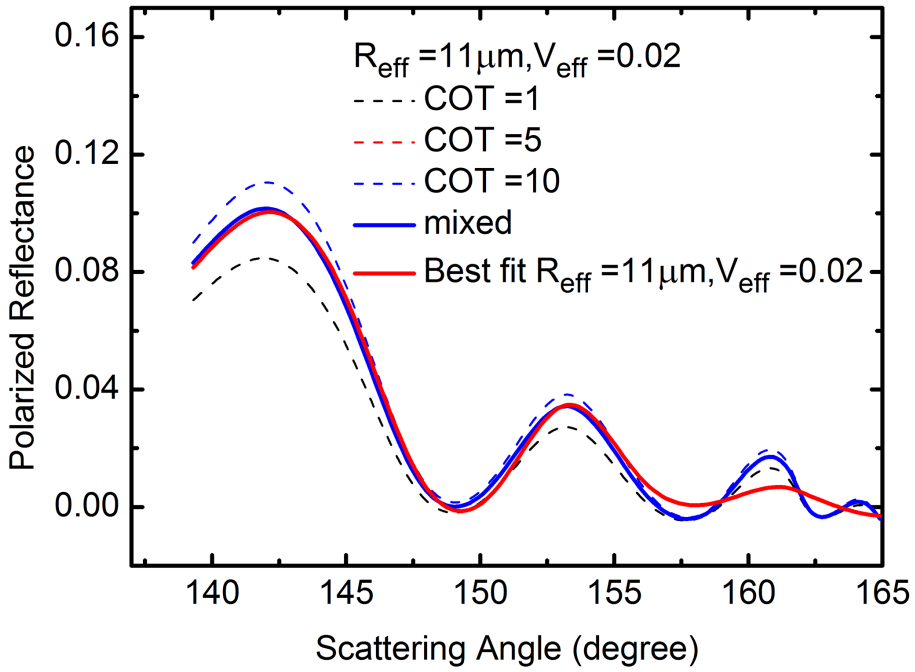


**Figure 3.** The retrievals from a heterogeneous cloud field with constant CDR = 11 μm and EV = 0.02 and three equal-area parts with COT = 1, 5 and 10. The black, blue and red dashed lines indicate the separate rainbow structure for sub-scale cloud fields with COT = 1, 5 and 10, respectively; the blue line is the rainbow structure for the heterogeneous cloud field; the red line represents the best fit.





AMTD
8, 6559–6597, 2015



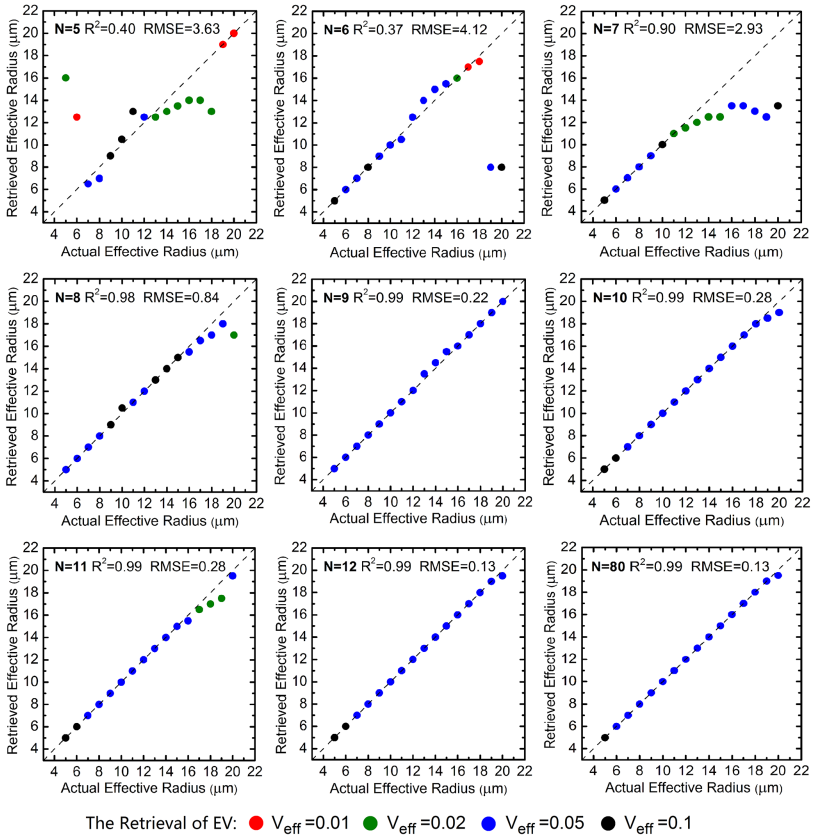


**Figure 4.** Comparisons of the retrieved CDR and EV with the actual values assumed in the RT3 modeling. In all cases, the actual EV and the COT were assumed to be 0.05 and 5, respectively. *N* in every plot represents the number of POLDER-like reflectances employed in the inversion. From top-left to bottom-right, *N* increases from 5 to 12, *N* = 80 is given at last. The color of the points represents the EV results.





AMTD
8, 6559–6597, 2015

A better understanding of POLDER's cloud droplet size retrieval

H. Shang et al.



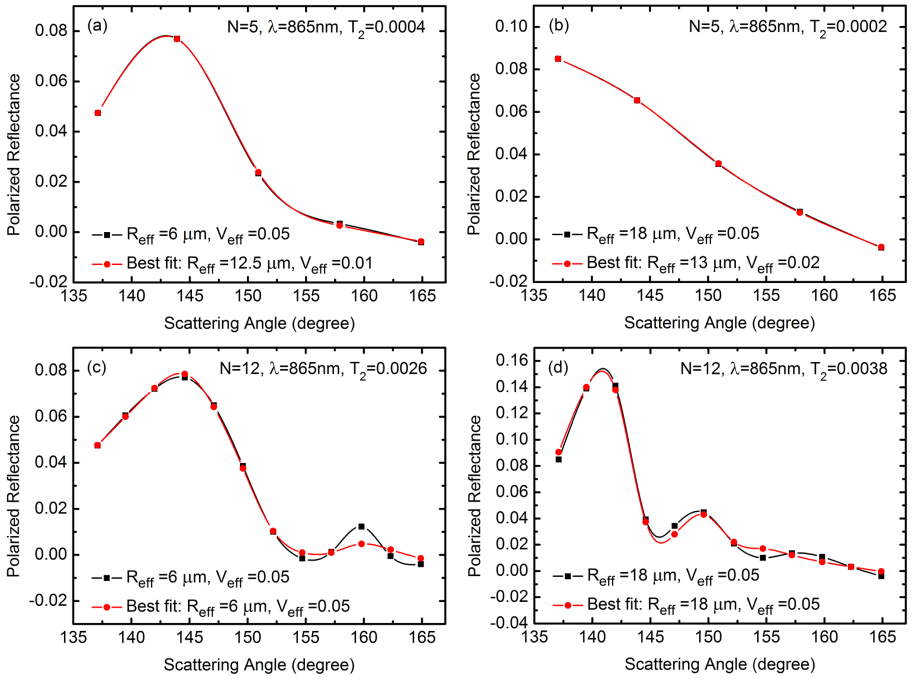


**Figure 5.** Comparisons of the observed rainbow structure and best fit curves when $N = 5$ and $N = 12$. The black and red points are the model (POLDER-like) and best fit reflectances, respectively. The COT was assumed to be 5 in all cases.





AMTD
8, 6559–6597, 2015

A better understanding of POLDER's cloud droplet size retrieval

H. Shang et al.



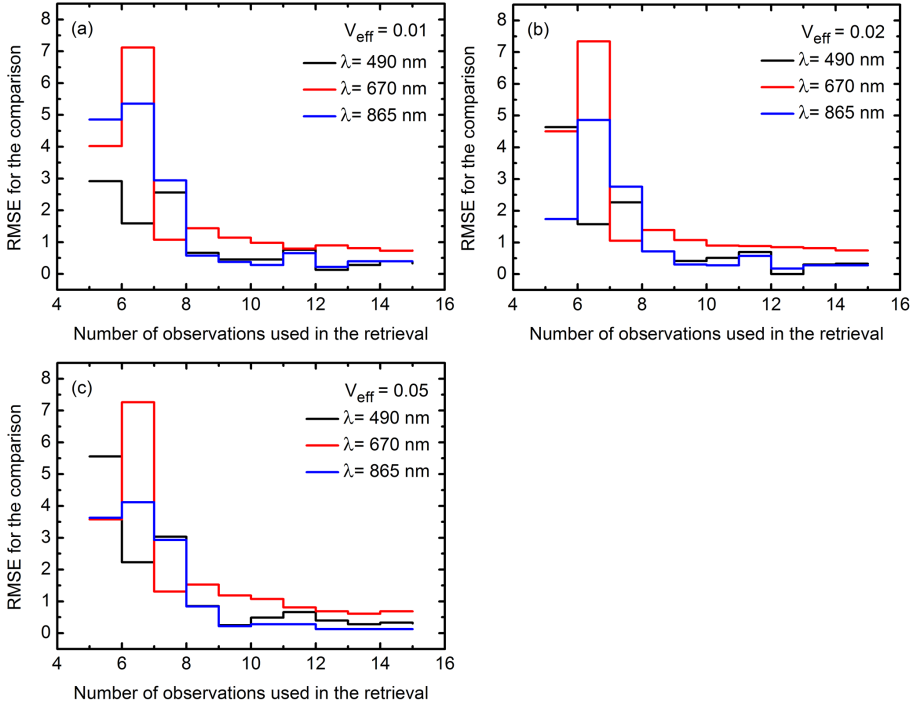


**Figure 6.** Comparisons of RMSE for the CDR retrievals using different numbers of observations at wavelengths of 490, 670 and 865 nm and for EVs of 0.01, 0.02 and 0.05, respectively. The COT was assumed to be 5 in all cases.





AMTD
8, 6559–6597, 2015



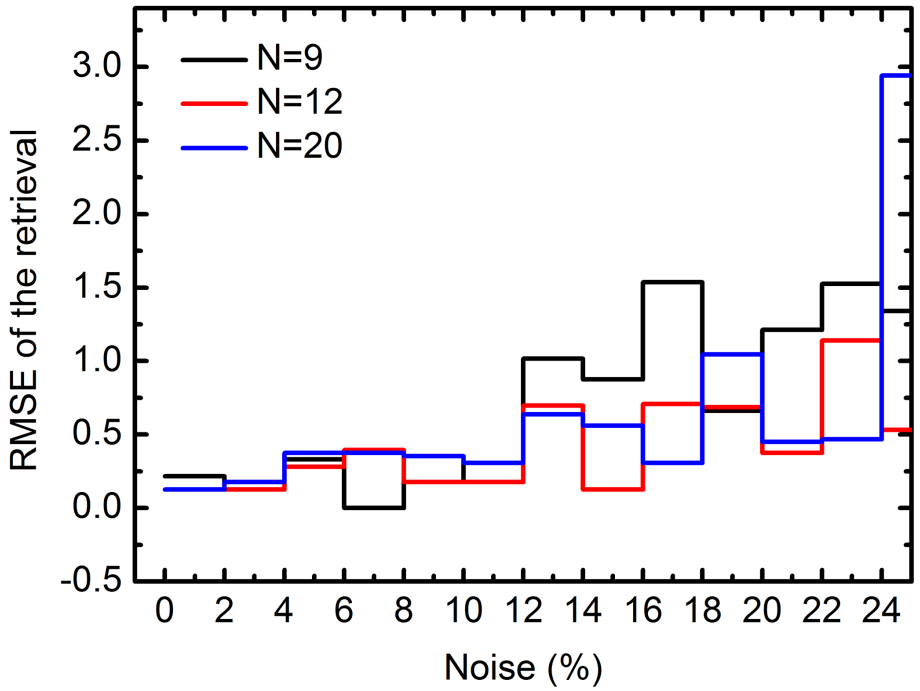


**Figure 7.** Dependence of RMSE for CDR estimation on noise level when 9, 12 and 20 observations are adopted in the retrieval. The percentage of noise represents the standard deviation of the Gaussian noise added on the simulated measurements. In all cases, the EV and COT were assumed to be 0.05 and 5 in all cases, respectively.





AMTD
8, 6559–6597, 2015



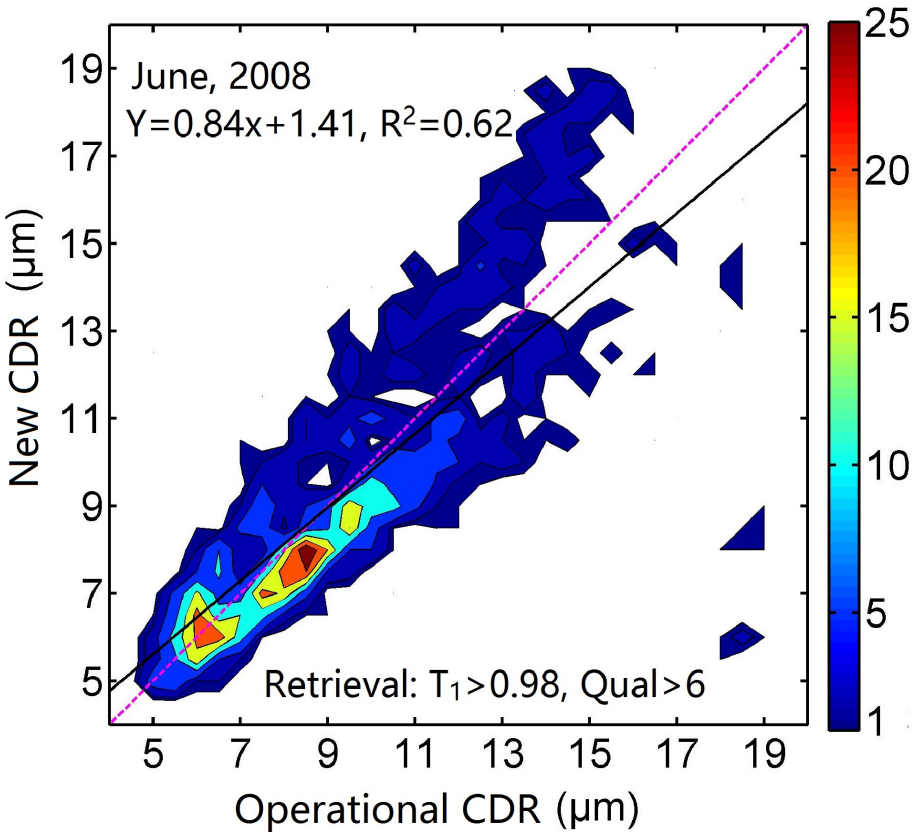


**Figure 8.** Comparisons between the CDRs estimated from our method and operational procedure. The global POLDER L1B data in June 2008 were used; the results were determined using the following criteria: $T_1 > 0.98$ and Qual > 6.





AMTD
8, 6559–6597, 2015



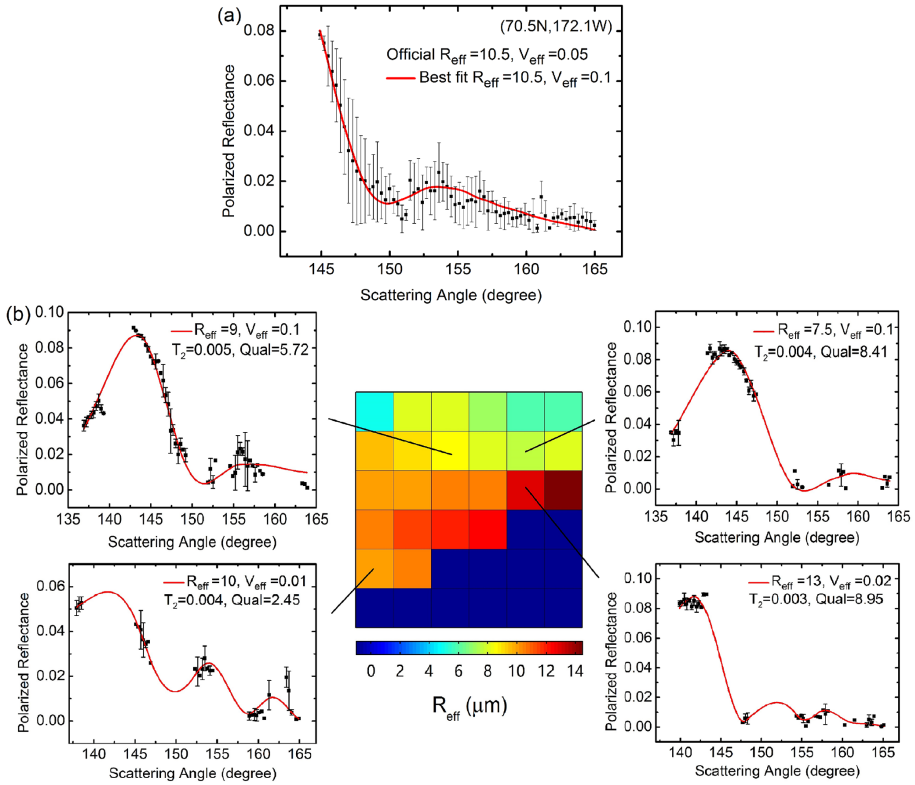


**Figure 9.** Sub-scale CDR and EV estimates from POLDER L1B data for 1 June 2008. The CDR retrieval for 70.5° N, 172.1° W with a resolution of 150 km × 150 km is shown in **(a)**; the CDR and EV estimates are comparable to the POLDER size distribution products. We divided the square in **(a)** into 36 sub-squares and retrieved corresponding CDR and EV values at a resolution of 7 × 7 pixels, The CDR distributions and fitting curves for the sub-squares are shown in **(b)**; the dark blue color represents a lack of valid retrievals.





AMTD
8, 6559–6597, 2015

A better understanding of POLDER's cloud droplet size retrieval

H. Shang et al.